Available online at www.sciencedirect.com

ScienceDirect

Proceedings of the Combustion Institute 39 (2023) 5591–5599

Proceedings of the Combustion Institute

www.elsevier.com/locate/proci

Pore-scale study of coke formation and combustion in porous media using lattice Boltzmann method

Timan Lei, Kai H. Luo*

Department of Mechanical Engineering, University College London, Torrington Place, London WC1E 7JE, United Kingdom

Received 5 January 2022; accepted 5 September 2022
Available online 9 November 2022

Abstract

In-situ combustion (ISC) has long been recognized as a promising technique for heavy oil recovery. However, ISC includes multiple physicochemical processes, which are still poorly understood and difficult to predict and control. This study establishes a lattice Boltzmann (LB) model to simulate the two important aspects of ISC at the pore scale: coke formation and combustion. The LB model includes thermal expansion effects and solves the reactive air-coke interface without iterations. Moreover, this model improves upon previous models by considering both coke formation and two-step coke combustion, as well as the growth of solid geometry. Results show that the LB model correctly captures coke combustion properties. Meanwhile, the newly introduced coke formation and two-step combustion yield important findings. As heat released from combustion transfers downstream, oil cracking and coke formation ahead of the combustion front are successfully tracked. The generated coke fuels the upstream combustion, making the system self-sustained. During coke formation and combustion, four coke transition states are identified. In addition, a parametric study demonstrates that the large inlet oxygen content and driving force are desirable, while too high a driving force should be avoided as it causes high burning temperature. Furthermore, it suggests that the inlet air temperature should be set appropriately. On one hand, a high temperature may promote coke formation and retard the front propagation. On the other hand, a low temperature may slow down the combustion of coke 2, even though it is high enough to ensure the ignition of coke 1. The decelerated coke 2 combustion may further cause the insufficient heat release and the failed coke formation, thus inducing the early termination of combustion. Such effects of the inlet temperature indicate the necessity of considering coke formation and two-step coke combustion. These results help to improve the understanding and facilitate the development of ISC.

Keywords: Two-step coke combustion; Coke formation; Lattice boltzmann method; Porous media; Pore scale

* Corresponding author.
E-mail addresses: k.luo@ucl.ac.uk, prof.k.h.luo@outlook.com (K.H. Luo).

https://doi.org/10.1016/j.proci.2022.09.053

1. Introduction

As the conventional light oil sources are being exhausted, extensive attention is being focused on the recovery of heavy oils. In-situ combustion (ISC), as an effective thermal recovery method, has long been of interest [1]. In a typical ISC process, hot air is injected to oxidize hydrocarbons (or coke) in oil reservoirs, forming a combustion front. From such a front, significant heat is released to increase the oil temperature and the driving energy. This contributes to improving the oil mobility and enhancing the recovery efficiency [2]. As heat from combustion transfers downstream, crude oils ahead of the combustion front crack into light oils and solid cokes that usually fuel the combustion process [3]. ISC is thus self-sustained and can efficiently drain oils with improved mobility towards production wells [4]. Although ISC is a promising technique in theory and has achieved some successes in industry, it is generally hard to predict and control. This mainly stems from the fact that reactions involved in ISC are complex, strongly coupled, and not well understood [1,5]. Therefore, to improve the development of ISC, it is necessary to model and understand the fundamental reaction dynamics.

In a successful ISC process, the two important reactions are coke formation (or oil cracking) and coke combustion [5,6]. These two reactions bring in complex phenomena, like unsteady fluid flow, reactive fluid-solid interface, conjugate heat transfer, compressible gas, and variable solid geometry. Some numerical and experimental works have been conducted to study these processes and enrich the knowledge base of ISC. For instance, a flood-pot technique was applied to experimentally determine the available coke for combustion and the required air from injection. Results demonstrated the available coke varied with oil properties, porous medium structures, and air flux [7]. Experiments were also conducted in pyrolysis and combustion reactors to investigate the coke formation process. The generated coke was found to be controlled by the conversion of crude oils and operation conditions [8]. In parallel, numerical models were built to study reactions involved in ISC. As one of the pioneering works, Belgrave et al. [9] proposed a unified pseudo-mechanistic reaction model to study ISC. They grouped the hydrocarbons based on their reaction mechanisms and captured the main crude oil transformations. This model has been widely accepted and taken as a starting point by the following researchers. For example, an upscaling methodology for field-scale reaction was built and the modeling results suggested heat conduction could stabilize the coke combustion front [10]. A one-dimensional model was built to analyse ISC, with both pyrolysis and vaporization being included. This model distinguished three pseudo-components in oil, ignored the oil mobility, and simplified coke as C [11]. More recently, models were developed for evaluating influencing factors of ISC, like the vapor-liquid equilibrium behavior, the injected air properties, and the porous medium characteristics [12,13].

Existing results have improved the understanding of ISC, including main reactions (i.e., coke formation and combustion) and effects of key factors. They however described reactions in porous oil reservoirs at macroscopic scales and applied volume-averaged techniques without considering pore-scale details. On the other hand, empirical correlations that depend on pore-scale structures are required to estimate effective parameters [3,14]. Thus, models that can provide pore-scale details of coke formation and combustion during ISC are desirable.

As a powerful solver for porous media flows at the pore scale, the lattice Boltzmann (LB) method has been developed over the past three decades [15,16]. To simulate the complex physicochemical processes involved in ISC, some LB simulations have been reported. Kang et al. [17–19] and Zhang et al. [20] developed LB boundary schemes to accurately model the species conservation condition at the reactive fluid-solid interface. In these simulations, Kang et al. proposed a volume of pixel scheme to track the porous structure evolutions, including both solid dissolution and formation. Meanwhile, LB models with a half-lattice division scheme or additional source terms were developed to implement the conjugate heat transfer among different phases, without conventional extrapolations or iterations [21,22]. As for combustion simulations, several efforts have been made over the past years. Yamamoto et al. [23,24] developed an LB model for propane combustion and further simulated soot combustion, which however ignored thermal expansion effects. To fill this gap, Lin and Luo [25,26] proposed a discrete Boltzmann model to study subsonic and supersonic combustion phenomena, as well as nonpremixed and partially premixed reactive flows. Meanwhile, based on the low-Mach approximation, LB simulations were carried out to model the combustion of low-speed flows. In these models, the thermal compressibility was included by modifying equilibrium distribution functions [27] or combining finite difference schemes [28]. Recently, to further account for solid combustion, Liu et al. [29] developed an LB model for char-pellet combustion, with the sodium release and ash inhibition effects on oxygen diffusion being considered.

On the basis of these works, Xu et al. [3] proposed a pore-scale LB model to investigate coke combustion front properties. They distinguished different combustion regimes and suggested the diffusion-limited one was desirable in industrial applications. However, an iteration scheme was required to model the air-coke interface, which was

hard to implement and computationally demanding. Besides, variations in air density caused by thermal expansion were not considered. For these reasons, we recently proposed a new pore-scale multiple-relaxation time (MRT) LB model to simulate solid coke combustion [30]. This new model includes thermal expansion effects and avoids iteration calculations. Our results captured coke combustion properties and assessed influencing factors. This first-step work however has some limitations: coke formation is not considered, coke combustion is simplified as a one-step reaction, thermal effects on air properties (like viscosity, mass diffusivity, and heat diffusivity) are ignored. To overcome these shortcomings, this study further modifies and improves our recent LB model to simulate coke formation and combustion during the ISC process.

2. Mathematical model

The formation and combustion of solid coke during ISC are investigated in a porous medium, where the solid matrix (an assembly of solid mineral grains) is unreactive and pore spaces are filled with inert gas and oil components. Initially, limited solid mineral grains are coated by coke and the compressible hot air at temperature T_0 is injected by a driving force $\boldsymbol{F} = (F_x,\ F_y)$. Once oxygen ($O_2$) from air comes into contact with coke, coke combustion takes place at the air-coke interface, which is described by two sequential reactions [10,29],

$$C_1 + a_1O_2 \rightarrow b_1CO + c_1CO_2 + C_2 + Q_1, \tag{1}$$

$$C_2 + a_2O_2 \rightarrow b_2CO + c_2CO_2 + Q_2. \tag{2}$$

Here, two types of coke are considered: coke 1 (C_1) and coke 2 (C_2). After ignition, the combustion front propagates forward and significant heat is released to increase the downstream temperature. Consequently, oils on the downstream side become heated and crack into light oils and solid C_1. The produced C_1 deposited on solid grains can fuel the upstream combustion. Coke formation is simplified as [9,10],

$$\text{Heavy oil} + Q_3 \rightarrow \text{Light oil} + C_1, \tag{3}$$

For the above coke formation and combustion, reaction rates at temperature T are estimated according to the first-order Arrhenius-type equation as [23],

$$Fr_\kappa = \omega_\kappa C^I_{O_2} = A_\kappa \exp(-E_\kappa/RT) C^I_{O_2}, \tag{4}$$

$$Fr_3 = \omega_3 C^I_o = A_3 \exp(-E_3/RT) C^I_o, \tag{5}$$

where $\kappa = 1, 2$ stands for reactions (1) and (2). $A_{1,2,3}$, $E_{1,2,3}$, and R are the pre-exponential factor, the activation energy, and the ideal gas constant, respectively. $C^I_{O_2}$ and C^I_o are molar concentrations of O_2 and oil components at interface I, respectively. The interface I represents air-C_1, air-C_2, and oil-C_1/grain for reactions (1)–(3), respectively.

For coke combustion (1)- (2), both carbon monoxide (CO) and carbon dioxide (CO_2) are considered as reaction products. The CO/CO_2 mole ratio at temperature T is determined by [29],

$$Np_\kappa = b_\kappa/c_\kappa = A_p \exp(-E_p/RT), \tag{6}$$

where A_p and E_p are two empirical parameters. The heat released from combustion (Q_κ) and required for oil cracking (Q_3) are calculated by,

$$Q_{1,2,3} = Fr_{1,2,3} hr_{1,2,3}, \tag{7}$$

with $hr_{1,2,3}$ being the chemical reaction heat. As coke burns out or accumulates gradually, the update of solid geometry is tracked by [18],

$$\partial_t V_{c1} = S_c V_m (Fr_3 - Fr_1), \tag{8}$$

$$\partial_t V_{c2} = S_c V_m (Fr_1 - Fr_2), \tag{9}$$

where V_{c1} and V_{c2} are volumes of C_1 and C_2, respectively, V_{cm} is the molar coke volume, and S_c is the reactive surface area.

During coke combustion, fluid flow is assumed to satisfy the low Mach number condition and fluid density varies as a consequence of temperature change. In addition, as explained in [11], the mobility of solid phases (coke and solid matrix) and oil components is sufficiently small and can be ignored. Based on these simplifications, a constant oil concentration ahead of the combustion front is applied. Governing equations for air flows in pore spaces and heat transfer in both pore spaces and solid phases are built as,

$$\partial_t \rho_g + \nabla \cdot (\rho_g \boldsymbol{u}) = 0, \tag{10}$$

$$\partial_t (\rho_g \boldsymbol{u}) + \nabla \cdot (\rho_g \boldsymbol{uu}) = -\nabla p + \nabla \cdot (\nu \rho_g \nabla \boldsymbol{u}) + \boldsymbol{F}, \tag{11}$$

$$\partial_t (\rho_g Y_n) + \nabla \cdot (\rho_g Y_n \boldsymbol{u}) = \nabla \cdot (D_n \rho_g \nabla Y_n), \tag{12}$$

$$\partial_t (\rho c_p T) + \nabla \cdot (\rho c_p T \boldsymbol{u}) = \nabla \cdot (\alpha \rho c_p \nabla T) + Q, \tag{13}$$

where $\boldsymbol{u}$, ρ_g, p, and ν are the gas velocity, density, pressure, and kinematic viscosity, respectively. ρ, c_p, α, and $k = \alpha \rho c_p$ in Eq. (13) are the local density, specific heat at constant pressure, thermal diffusivity, and thermal conductivity, respectively. These four parameters for the gas and solid phases are noted by subscripts g and s, respectively. Y_n and D_n are the mass fraction and diffusion coefficient of species n ($n = O_2, CO_2, CO$), respectively. Y_n is related to the molar concentration as, $C_n = Y_n \rho_g / M_n$, with M_n being the molecular weight. Effects of temperature variations on air properties are estimated as [31,32],

$$\mu = \mu' (T/T')^{0.69}, \quad D_n = D'_n (T/T')^{1.5}, \tag{14}$$

where $\mu = \rho_g \nu$ is the air dynamic viscosity and the superscript $'$ represents reference conditions.

Coke formation and combustion reactions at interface I is described by boundary conditions for the species conservation, the conjugate heat transfer, and the no-slip velocity as [3,18],

$$\boldsymbol{n} \cdot D_n \rho_g \nabla Y_n^I = \sum \varsigma_{1,2,3} Fr_{1,2,3} M_n, \tag{15}$$

$$\begin{aligned} &T^{I,+} = T^{I,-}, \\ &\boldsymbol{n} \cdot (k \nabla T)^{I,+} = \boldsymbol{n} \cdot (k \nabla T)^{I,-} + q, \end{aligned} \tag{16}$$

$$\boldsymbol{u}^I = (0,\ 0), \tag{17}$$

where $\boldsymbol{n}$ is the interface normal pointing to the gas phase, + and - denote parameters on either side of I, q is the heat flux caused by coke combustion, and ς is the stoichiometric coefficient. By introducing the characteristic length L, velocity U, and density ρ_{ch}, dimensionless parameters are derived as,

$$\boldsymbol{F}^* = \frac{\boldsymbol{F}}{\rho_{ch} U^2 / L},\ \mathrm{Re} = \frac{LU}{\nu},\ \mathrm{Pe}_n = \frac{LU}{D_n},\ \mathrm{Pr} = \frac{\nu}{\alpha_g}. \tag{18}$$

$\boldsymbol{F}^*$, Re, Pe_n, and Pr are the dimensionless force, the Reynolds number, the Peclet numbers, and the Prandtl number, respectively.

3. Numerical method

To solve the above governing Eqs (10)–(13), a two-dimensional nine-velocity (D2Q9) MRT LB model is developed [16]. Due to the uniform thermophysical properties and the thermal expansion effects, Eqs. (12)-(13) are firstly derived as [30],

$$\partial_t Y_n + \nabla \cdot (Y_n \boldsymbol{u}) = \nabla \cdot (D_n \nabla Y_n) + F_n, \tag{19}$$

$$\partial_t T + \nabla \cdot (T \boldsymbol{u}) = \nabla \cdot (\alpha \nabla T) + F_T, \tag{20}$$

with source terms F_n and F_T being,

$$\begin{aligned} &F_n = \tfrac{D_n}{\rho_g} \nabla Y_n \cdot \nabla \rho_g + Y_n \nabla \cdot \boldsymbol{u}, \\ &F_T = \tfrac{Q}{\rho c_p} + \tfrac{\nabla (\rho c_p)}{\rho c_p} \cdot (\alpha \nabla T - T \boldsymbol{u}) - \tfrac{T \partial_t (\rho c_p)}{\rho c_p}. \end{aligned} \tag{21}$$

Note that values of c_p are set as constants for both gas and solid phases in this study. Thus, in non-reactive solid and gas areas, the above calculation expression for F_T can be further simplified as, $F_T = Q/\rho c_p + \alpha \nabla T \cdot \nabla (\rho c_p)/\rho c_p + T \nabla \cdot \boldsymbol{u}$.

Three sets of evolution equations are built in the proposed LB model as [30],

$$\begin{aligned} &f_i(\boldsymbol{x} + \boldsymbol{e}_i \delta_t,\ t + \delta_t) - f_i(\boldsymbol{x},\ t) \\ &= -\left(\boldsymbol{M}^{-1} \boldsymbol{S} \boldsymbol{M}\right)_{ij} \left[f_j(\boldsymbol{x},\ t) - f_j^{eq}(\boldsymbol{x},\ t)\right] \\ &\quad + \delta_t \left(\boldsymbol{M}^{-1} (\boldsymbol{I} - 0.5\boldsymbol{S}) \boldsymbol{M}\right)_{ij} \left(\overline{F}_j + \overline{C}_j\right), \end{aligned} \tag{22}$$

$$\begin{aligned} &g_{n,i}(\boldsymbol{x} + \boldsymbol{e}_i \delta_t,\ t + \delta_t) - g_{n,i}(\boldsymbol{x},\ t) \\ &= g_{n,i}(\boldsymbol{x} + \boldsymbol{e}_i \delta_t,\ t + \delta_t) - g_{n,i}(\boldsymbol{x},\ t) \\ &= -\left(\boldsymbol{M}^{-1} \boldsymbol{S}_n \boldsymbol{M}\right)_{ij} \left[g_{n,j}(\boldsymbol{x},\ t) - g_{n,j}^{eq}(\boldsymbol{x},\ t)\right] \\ &\quad + \delta_t \overline{F}_{n,i} + 0.5 \delta_t^2 \partial_t \overline{F}_{n,i}, \end{aligned} \tag{23}$$

$$\begin{aligned} &h_i(\boldsymbol{x} + \boldsymbol{e}_i \delta_t,\ t + \delta_t) - h_i(\boldsymbol{x},\ t) \\ &= -\left(\boldsymbol{M}^{-1} \boldsymbol{S}_t \boldsymbol{M}\right)_{ij} \left[h_j(\boldsymbol{x},\ t) - h_j^{eq}(\boldsymbol{x},\ t)\right] \\ &\quad + \delta_t \overline{F}_{T,i} + 0.5 \delta_t^2 \partial_t \overline{F}_{T,i}, \end{aligned} \tag{24}$$

for $i, j = 0, 1, \ldots, 8$, where $f_i(\boldsymbol{x},\ t)$, $g_{n,i}(\boldsymbol{x}, t)$, and $h_i(\boldsymbol{x}, t)$ are distribution functions for the density, the mass fraction of species n, and the temperature fields, respectively. The corresponding equilibrium distribution functions are f_i^{eq}, $g_{n,i}^{eq}$, and h_i^{eq}, respectively. $\overline{F}_i$, $\overline{F}_{n,i}$, and $\overline{F}_{T,i}$ are distribution functions for the driving force ($\boldsymbol{F}$) and source terms (F_n, F_T), respectively. $\overline{C}_j$ is the correction term to eliminate the deviation from third-order velocity moments. The transformation matrix $\boldsymbol{M}$ can map distribution functions from the physical space $\boldsymbol{\psi}$ to the moment space as $\hat{\boldsymbol{\psi}} = \boldsymbol{M} \cdot \boldsymbol{\psi}$. $\boldsymbol{S}$, $\boldsymbol{S}_n$, and $\boldsymbol{S}_t$ are the diagonal relaxation matrices of relaxation rates in the moment space. The macroscopic variables can be obtained from the distribution functions as,

$$\begin{aligned} &\rho = \sum_i f_i, \quad \rho \boldsymbol{u} = \sum_i \boldsymbol{e}_i f_i + 0.5 \delta_t \boldsymbol{F}, \\ &Y_n = \sum_i g_{n,i}, \quad T = \sum_i h_i. \end{aligned} \tag{25}$$

The equation of state to relate the gas pressure and temperature is defined as, $p = \rho \sum R Y_n T / M_n$.

Coke formation and combustion reactions are implemented by solving boundary conditions (Eqs. (15)–(17)). On one hand, the conjugate heat transfer (Eq. (16)) is automatically realized by solving Eq. (13) [30]. On the other hand, to solve Eqs. (15) and (17), the interface mass fraction Y_n^I is firstly determined via the finite-difference scheme as [20],

$$\boldsymbol{n} \cdot \nabla Y_n^I = \left(Y_n^g - Y_n^I\right)/d_c,\ d_c = 0.5 \boldsymbol{n} \cdot \boldsymbol{e}_i \delta_x, \tag{26}$$

where Y_n^g is the species mass fraction at the gas node neighboring I and $\boldsymbol{e}_i$ is the discrete velocities. By inserting Eq. (26) into Eq. (15), Y_n^I is calculated as,

$$Y_{\mathrm{O}_2}^I = \frac{D_{\mathrm{O}_2} Y_{\mathrm{O}_2}^g}{D_{\mathrm{O}_2} - d_c \sum a_\kappa \omega_\kappa}, \tag{27}$$

$$Y_\zeta^I = Y_\zeta^g - \frac{d_c \sum \varsigma_\kappa \omega_\kappa Y_{\mathrm{O}_2}^I M_\zeta}{D_\zeta M_{\mathrm{O}_2}}, \tag{28}$$

$$C_o^I = \frac{D_{\mathrm{Oil}} C_o^g}{D_{\mathrm{Oil}} - d_c \omega_3}, \tag{29}$$

with $\zeta = \mathrm{CO}_2,\ \mathrm{CO}$. The halfway bounce-back scheme is chosen to realize this reactive boundary with no-slip velocity and given mass fractions.

To track solid geometry variations with coke formation and combustion, the volume of pixel scheme is applied [17]. Explicitly, the lattice grid

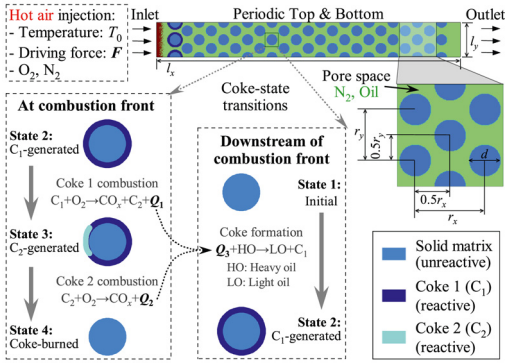

Fig. 1. Schematic of the problem: coke formation and combustion in porous media.

size is assumed to be fine enough and thus each solid grid represents only one material η ($\eta = C_1, C_2$, solid matrix), but allows other minerals to deposit. For a solid grid of η, the initial solid volume is set as $V_{\eta,0}$ and the volume is updated at each time step via Eqs. (8)-(9). On one hand, when the solid volume doubles ($V_\eta = 2V_{\eta,0}$), one of the neighboring nodes changes to a solid node of η, with the ratio of precipitation probability between the nearest node and diagonal nodes being 4 : 1. On the other hand, when the solid volume becomes zero ($V_\eta = 0$), the node degrades to a gas node from C_2 or a C_2 node from C_1. More details about the proposed MRT LB model are provided in the Supplementary Material.

4. Results and discussion

The developed LB model is applied to simulate the two critical aspects for a successful ISC process: coke formation and combustion in porous media. As displayed in Fig. 1, a porous structure with porosity $\phi = 0.57$ and initial C_1 volume fraction $\phi_{c1,0} = 0.017$ is constructed [33]. Geometric parameters of the medium are $l_x = 552$ μm, $l_y = 64$ μm, $d = 20$ μm, $r_x = 44$ μm, and $r_y = 32$ μm. This medium is initially filled with hot nitrogen and oil components at temperature T_0. The compressible hot air at temperature T_0, density $\rho_{g,0}$, and O_2 mass fractions $Y_{O_2,0}$ is injected to react with coke by a driving force $\boldsymbol{F} = (F_x, 0)$. In the subsequent simulations, reaction parameters are, $A_1 = 3.21 \times 10^7$ m/s, $E_1 = 136.9$ kJ/mol, $hr_1 = 388.5$ kJ/mol; $A_2 = 1.1 \times 10^7$ m/s, $E_2 = 131.09$ kJ/mol, $hr_2 = 500$ kJ/mol; $A_3 = 4.06 \times 10^9$ m/s, $E_3 = 177.2$ kJ/mol, $hr_3 = 37.97$ kJ/mol; and $R = 8.314$ J/molK [3,9,11,29,34,35]. The system pressure keeps unchanged as $p = 1$ Mpa. Thermophysical properties of solid phases (i.e., C_1, C_2, and solid matrix) are fixed as, $c_{p,s} = 0.72$ kJ/kgK, $\rho_s = 2260$ kg/m^3, $k_s = 4.14$ J/smK,

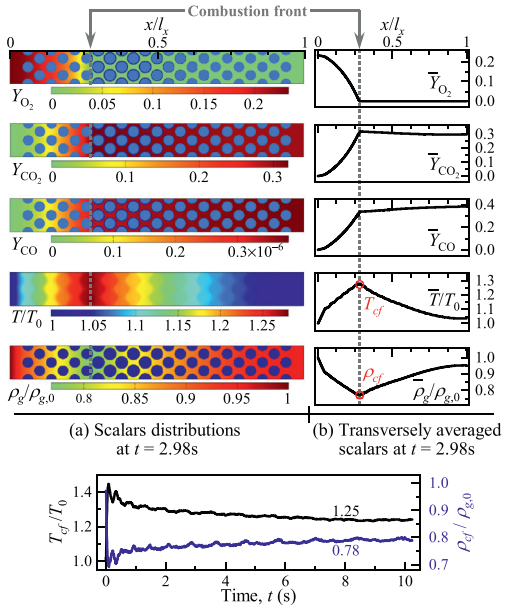

Fig. 2. Coke combustion and formation properties in the base case: (a) Distributions of mass fractions (Y_{O_2}, Y_{CO_2}, Y_{CO}), temperature (T), and air density (ρ_g) at $t = 2.98$ s. (b) Transversely averaged scalars. (c) Temporal evolutions of combustion front temperature (T_{cf}) and density (ρ_{cf}).

$\alpha_s = 2.55 \times 10^{-6}$ m^2/s; while those of the gas phase vary with temperature. Specifically, ρ_g is obtained by solving LB equations, ν and D_n are calculated by Eq. (14), and α_g is determined by a fixed Pr = 0.72. The reference conditions for Eq. (14) are, $T' = 293$ K, $\mu' = 1.84 \times 10^{-5}$ kg/ms, $D_{O_2} = 1.76 \times 10^{-6}$ m^2/s, $D_{CO_2} = 1.6 \times 10^{-6}$ m^2/s, $D_{CO} = 2.08 \times 10^{-6}$ m^2/s, $D_{Oil} = 5.0 \times 10^{-9}$ m^2/s. Note that $c_{p,g}$ is fixed as $c_{p,g} = 1.09$ kJ/kgK since it varies with T slightly. The conversion between physical and lattice units is based on Eq. (18), with the characteristic parameters being $L = d$, $U = \alpha_g/L$, and $\rho_{ch} = \rho_{g,0}$. After grid convergence tests, a mesh of size $N_x \times N_y = 1656 \times 192$ is used to cover the porous medium. Zero-gradient conditions are applied at the outlet and the top and bottom are periodic. Coke formation and combustion properties and effects of key parameters in ISC are then investigated.

4.1. Coke formation and combustion characteristics

A base case with $F_x^* = 15$, $T_0 = 773$ K, and $Y_{O_2,0} = 0.233$ is firstly simulated. Figure 2(a) shows distributions of species mass fractions, temperature, and air density at $t = 2.98$ s. Injected O_2 flows through pore spaces to oxidize solid coke at the air-coke interface, forming the combustion front area. At this front, O_2 and coke are exhausted, while CO

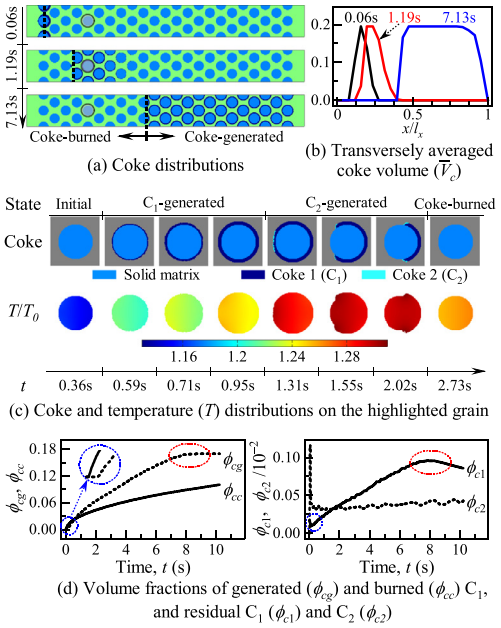

Fig. 3. Coke evolutions in the base case: (a) Coke distributions. (b) Transversely averaged coke volume ($\overline{V}_c$). (c) Coke and temperature (T) distributions during coke formation and combustion on the grain highlighted in (a). (d) Temporal evolutions of coke volume fractions: ϕ_{cg} and ϕ_{cc} for the generated and burned C_1; and ϕ_{c1} and ϕ_{c2} for the residual C_1 and C_2.

and CO_2 are generated. Such a combustion process releases heat, which makes temperature increase towards the front and reach a peak value there. Due to thermal expansion effects, air density varies in an opposite tendency and drops to a valley value at the combustion front. These observations are quantitatively verified by transversally averaged values (denoted by the superscript $\bar{}$) in Fig. 2(b). In addition, the temperature (T_{cf}) and air density (ρ_{cf}) at the combustion front are recorded versus time in Fig. 2(c), showing an almost stable burning condition with $T_{cf}/T_0 \approx 1.25$ and $\rho_{cf}/\rho_{g,0} \approx 0.78$. Compared with the inlet state, T_{cf} and ρ_{cf} vary by 25% and 22%, respectively. This implies the necessity of considering thermal expansion effects. These results show the typical coke combustion properties in porous media, which are consistent with those in our recent paper [30].

On the other hand, due to the newly introduced coke formation and two-step coke combustion schemes, coke transitions and distributions become different from our recent work [30]. Figure 3(a) illustrates that, at the combustion front, C_1 is oxidized to produce C_2 and C_2 burns out soon after the generation. As combustion goes on, the combustion front proceeds downstream and divides the medium into two areas. The upstream side of front is the coke-burned zone, where two types of coke burn out. On the downstream side, coke formation takes place and the newly formed C_1 on solid matrix can fuel the upstream combustion. This area is thus defined as the coke-generated area. The transversely averaged coke volumes in Fig. 3(b) also show the coke formation and accumulation on the downstream side.

To visualize coke transitions during coke formation and combustion, temporal evolutions of the residual coke and temperature distributions on a single solid mineral grain are provided in Fig. 3(c), from which four coke-transition states are identified. First, at the initial state, the grain is relatively cold and no coke deposits on its surface. Then, as heat released from combustion transfers to increase the downstream temperature, heavy oils crack to generate solid C_1 on the grain surface. The grain thus transfers to the C_1-generated state, with the grain becoming heated and coated by C_1. After that, the combustion front moves to the grain and C_1 burns to produce C_2, hence the C_2-generated state. As the combustion continues, the grain temperature increases significantly and the two types of coke burn out finally. At last, the grain cools down and changes to the coke-burned state.

The coke formation and combustion are quantified by temporal evolutions of coke volume fractions in Fig. 3(d). Both the generated C_1 (ϕ_{cg}) and the burned C_1 (ϕ_{cc}) increase with time at first, indicating the on-going coke formation and combustion. Besides, ϕ_{cg} grows more quickly than ϕ_{cc}, which implies the coke formation rate is fast enough to sustain combustion. As time passes, ϕ_{cc} increases constantly while ϕ_{cg} gradually approaches a stable value (marked by a red circle). This suggests the formed amount of coke reaches the system limit and thus coke formation stops finally. In addition, the enlarged initial period (marked by a blue circle) shows that coke combustion starts earlier than coke formation. This is because coke formation can be triggered only after significant heat released from combustion transfers to heat up the dowmstream side. To quantify coke transitions, the residual C_1 (ϕ_{c1}) and C_2 (ϕ_{c2}) volume fractions are also measured in Fig. 3(d). The curve of ϕ_{c1} decreases at first and increases after a short period (marked by a blue circle), which is caused by the quick coke combustion and the delayed coke formation. After an increasing period, ϕ_{c1} changes to decrease as coke formation stops (marked by a red circle). As for the residual C_2, ϕ_{c2} holds a relatively stable value. This verifies the above observation that C_2 burns out soon after its generation from the combustion of C_1.

4.2. *Effects of key parameters*

A series of simulation tests are conducted to evaluate the key parameters of ISC. To clarify sensitivities of coke formation and combustion, temporal evolutions of combustion front temperature

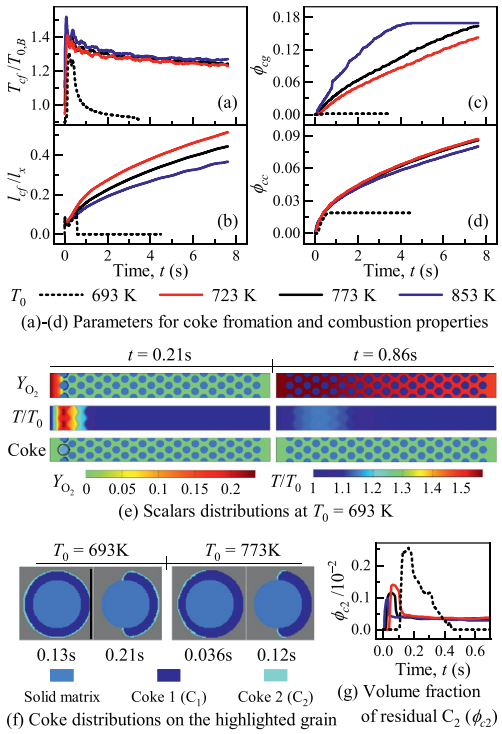

Fig. 4. Coke formation and combustion properties at different T_0: Temporal evolutions of (a) front temperature (T_{cf}), (b) front location (l_{cf}), (c) volume fraction of generated C_1 (ϕ_{cg}), (d) volume fraction of burned C_1 (ϕ_{cc}). (e) Distributions of O_2 mass fraction (Y_{O_2}), temperature (T), and coke at $T_0 = 693$ K. (f) Coke distributions on the grain highlighted in (e) at $T_0 = 693$, 773K. (g) Temporal evolutions of coke volume fractions of residual C_2 (ϕ_{c2}).

(T_{cf}) and location (l_{cf}), as well as generated C_1 (ϕ_{cg}) and burned C_1 (ϕ_{cc}) volume fractions are measured.

Simulations with different T_0 are firstly conducted to assess the influence of inlet air temperature. Obtained results are provided in Fig. 4, where T_{cf} is normalized by the inlet air temperature of the base case $T_{0,B} = 773$ K. Results for cases with $T_0 = 723, 773, 853$ K show that increasing T_0 affects the front temperature T_{cf} and the coke combustion (ϕ_{cc}) slightly (Figs. 4(a) and (d)). This can be explained by the limited O_2 for combustion [30]. However, the increase of T_0 retards the front propagation (l_{cf}) obviously (Fig. 4(b)), indicating it plays a negative role in ISC. The higher T_0 implies the more heat from combustion and also the less heat demand for triggering oil cracking. As shown in Fig. 4(c), this subsequently promotes coke formation on the downstream side. The combined effects of the enhanced coke formation and the almost unchanged coke combustion thus suppress the advance of the combustion front.

Different from the above three successful cases, curves of T_{cf}, ϕ_{cc}, and l_{cf} at $T_0 = 693$ K increase at first but stop growing after a short period, while

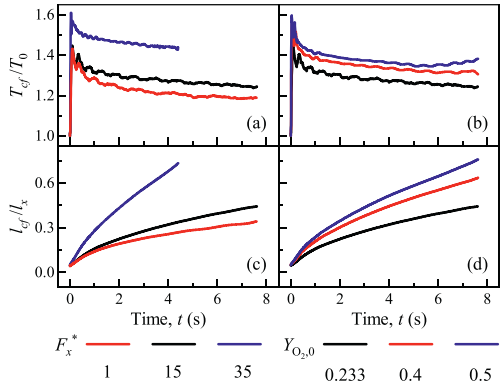

Fig. 5. Coke formation and combustion properties at different F_x^* and $Y_{O_2,0}$: Temporal evolutions of (a)-(b) front temperature (T_{cf}) and (c)-(d) front location (l_{cf}).

the curve of ϕ_{cg} remains zero (Figs. 4(a)-(d)). This suggests the ignition is successful but oil cracking is failed to be triggered. Thus, no coke is generated to sustain the combustion process and the system is terminated earlier than expected. This failed case is visualized by scalar distributions in Fig. 4(e). As can be seen, the system is not self-sustained and injected air breaks through the porous medium after the initial coke burns out. In addition, T_{cf} at $T_0 = 693$ K is smaller than other successful cases (Fig. 4(a)). This demonstrates the released heat from combustion is insufficient and thus the temperature rise is not enough to trigger oil cracking. To find out the cause of the insufficient heat, coke distributions on a single mineral grain are provided in Fig. 4(f). It is observed that, instead of burning out soon after generation, C_2 accumulates and covers C_1 at $T_0 = 693$ K. Temporal evolutions of residual C_2 (ϕ_{c2}) in Fig. 4(g) also show that the unburned C_2 at $T_0 = 693$ K is much higher than other cases. Such a slow combustion of C_2 causes the insufficient heat release and the failed coke formation. Therefore, T_0 should be large enough to ensure both the ignition and oil cracking, but a high T_0 should be avoided as it retards front propagation.

A sufficient amount of oxygen should be injected to sustain coke combustion during ISC, thus the inlet oxygen mass fraction ($Y_{O_2,0}$) and the driving force (F_x^*) are then investigated. Several simulations are carried out and parts of the results are shown in Fig. 5. It is obvious that the increasing $Y_{O_2,0}$ or F_x^* promotes coke formation and combustion, which leads to the improved front displacement efficiency. In the case with high $Y_{O_2,0}$, the available O_2 for combustion becomes sufficient and the combustion rate increases. Subsequently, more heat is released from combustion to trigger and boost oil cracking. Therefore, both coke formation and combustion are enhanced. In the case with large F_x^*, more O_2 is injected to react with coke,

which is thus similar to the case with large $Y_{O_2,0}$. It should be noted that however, the continuing increase of F_x^* may introduce the high burning temperature and thus should be avoided.

5. Conclusions

In this work, a new multiple-relaxation-time lattice Boltzmann (LB) model is developed for pore-scale simulations of coke formation and combustion during in-situ combustion (ISC) in porous media. This LB model considers both coke formation and two-step coke combustion, thus making advances over existing LB models. The reactions are modelled by solving the reactive air-coke interface, where species conservation and conjugate heat transfer conditions are implemented without iterations. Together with these reactions, pore-scale growth and degradation of the solid geometry are tracked by the volume of pixel scheme; variations of air properties (i.e., density, viscosity, and heat and mass diffusivities) with temperature are included. Simulation results reproduce the typical coke combustion properties. Furthermore, the coke formation process ahead of the combustion front is tracked for the first time. The generated coke 1 in the downstream area fuels the upstream combustion, which makes the system self-sustained. From temperature and coke distributions on a single solid mineral grain, four coke transition states are identified. A parametric study suggests the large driving force and inlet oxygen mass fraction can enhance the front propagation, but an excessive driving force should be avoided due to the high burning temperature. Besides, the inlet air temperature should be set appropriately. A high temperature may accelerate coke formation and suppress fluid flow and combustion front propagation. As for a low temperature, although it ensures the ignition of coke 1, it may slow down the combustion of coke 2 and decrease the heat release from combustion. Subsequently, this may cause insufficient temperature rise, unsuccessful oil cracking, and even early terminated combustion. As a whole, the improved LB model captures both coke formation and combustion properties, contributing to advancing the knowledge base of ISC.

Declaration of Competing Interest

There is no competing interest.

Acknowledgments

This work was supported by the UK Engineering and Physical Sciences Research Council under the projects “UK Consortium on Mesoscale Engineering Sciences (UKCOMES)” (Grant No EP/R029598/1) and “Mechanisms and Synthesis of Materials for Next-Generation Lithium Batteries Using Flame Spray Pyrolysis” (Grant No. EP/T015233/1). This work made use of computational support by CoSeC, the Computational Science Centre for Research Communities, through UKCOMES.

Supplementary materials

Supplementary material associated with this article can be found, in the online version, at doi:10.1016/j.proci.2022.09.053

References

[1] E.A. Araújo, A.A.R. Diniz, A.R. Gurgel, D.M.B.S. Lima, T.V. Dutra Jr, J.L.M. Barillas, Analysis of oil production by applying in situ combustion, Pet. Sci. Technol. 34 (1) (2016) 50–55.
[2] K. Guo, H.L. Li, Z.X. Yu, In-situ heavy and extra-heavy oil recovery: a review, Fuel 185 (2016) 886–902.
[3] Q.H. Xu, W. Long, H. Jiang, C. Zan, J. Huang, X. Chen, L. Shi, Pore-scale modelling of the coupled thermal and reactive flow at the combustion front during crude oil in-situ combustion, Chem. Eng. J. 350 (2018) 776–790.
[4] P.S. Sarathi, In-situ combustion handbook-principles and practices, Technical Report, National Petroleum Technology Office, Oklahoma, U.S., 1999.
[5] Y. Ren, N. Mahinpey, N. Freitag, Kinetic model for the combustion of coke derived at different coking temperatures, Energy Fuels 21 (1) (2007) 82–87.
[6] L.S. Gómex, Analysis of the in situ combustion process in a kinetic cell with optical access using computational fluid dynamics (CFD), Universidad Nacional de Colombia Sede Medellín, Medellín, Colombia, 2014 Ph.D. thesis.
[7] J.D. Alexander, W.L. Martin, J.N. Dew, Factors affecting fuel availability and composition during in situ combustion, J. Pet. Technol. 14 (10) (1962) 1154–1164.
[8] M. Ranjbar, Improvement of medium and light oil recovery with thermocatalytic in situ combustion, J. Can. Pet. Technol. 34 (08) (1995).
[9] J.D.M. Belgrave, R.G. Moore, M.G. Ursenbach, D.W. Bennion, A comprehensive approach to in-situ combustion modeling, SPE Advanced Technology Series 1 (01) (1993) 98–107.
[10] Z.Y. Zhu, Efficient simulation of thermal enhanced oil recovery processes, Stanford University, Stanford, California, USA, 2011 Ph.D. thesis.
[11] A.A. Mailybaev, J. Bruining, D. Marchesin, Analysis of in situ combustion of oil with pyrolysis and vaporization, Combust. Flame 158 (6) (2011) 1097–1108.
[12] D. Srinivasareddy, G.S. Kumar, A numerical study on phase behavior effects in enhanced oil recovery by in situ combustion, Pet. Sci. Technol. 33 (3) (2015) 353–362.
[13] H. Zheng, W.P. Shi, D. Ding, C.Y. Zhang, Numerical simulation of in situ combustion of oil shale, Geofluids 2017 (2017).
[14] Q.H. Xu, W. Long, H. Jiang, B. Ma, C. Zan, D.S. Ma, L. Shi, Quantification of the microstructure, effective hydraulic radius and effective transport proper-

ties changed by the coke deposition during the crude oil in-situ combustion, Chem. Eng. J. 331 (2018) 856–869.
[15] Q. Li, K.H. Luo, Q.J. Kang, Y.L. He, Q. Chen, Q. Liu, Lattice Boltzmann methods for multiphase flow and phase-change heat transfer, Prog. Energy Combust. Sci. 52 (2016) 62–105.
[16] Z.L. Guo, C. Shu, Lattice Boltzmann method and its applications in engineering, World Scientific Publisher, Singapore, Singapore, 2013.
[17] Q. Kang, P. Lichtner, D. Zhang, Lattice Boltzmann pore-scale model for multicomponent reactive transport in porous media, Journal of Geophysical Research: Solid Earth 111 (B5) (2006) B05203.
[18] Q.J. Kang, L. Chen, A.J. Valocchi, H.S. Viswanathan, Pore-scale study of dissolution-induced changes in permeability and porosity of porous media, J. Hydrol. 517 (2014) 1049–1055.
[19] L. Chen, Q.J. Kang, B. Carey, W.Q. Tao, Pore-scale study of diffusion-reaction processes involving dissolution and precipitation using the lattice Boltzmann method, Int. J. Heat Mass Transf. 75 (2014) 483–496.
[20] T. Zhang, B.C. Shi, Z.L. Guo, Z.H. Chai, J.H. Lu, General bounce-back scheme for concentration boundary condition in the lattice-Boltzmann method, Phys. Rev. E 85 (1) (2012) 016701.
[21] Y.L. He, Q. Liu, Q. Li, W.Q. Tao, Lattice Boltzmann methods for single-phase and solid-liquid phase-change heat transfer in porous media: a review, Int. J. Heat Mass Transf. 129 (2019) 160–197.
[22] H. Karani, C. Huber, Lattice Boltzmann formulation for conjugate heat transfer in heterogeneous media, Phys. Rev. E 91 (2) (2015) 023304.
[23] K. Yamamoto, X.Y. He, G.D. Doolen, Simulation of combustion field with lattice Boltzmann method, J. Stat. Phys. 107 (1–2) (2002) 367–383.
[24] K. Yamamoto, N. Takada, M. Misawa, Combustion simulation with lattice Boltzmann method in a three-dimensional porous structure, Proc. Combust. Inst. 30 (1) (2005) 1509–1515.
[25] C.D. Lin, K.H. Luo, L.L. Fei, S. Succi, A multi–component discrete Boltzmann model for nonequilibrium reactive flows, Sci. Rep. 7 (1) (2017) 1–12.
[26] C.D. Lin, K.H. Luo, Mesoscopic simulation of nonequilibrium detonation with discrete Boltzmann method, Combust. Flame 198 (2018) 356–362.
[27] Y. Feng, P. Sagaut, W. Tao, A three dimensional lattice model for thermal compressible flow on standard lattices, J Comput Phys 303 (2015) 514–529.
[28] S.A. Hosseini, H. Safari, N. Darabiha, D. Thévenin, M. Krafczyk, Hybrid lattice Boltzmann-finite difference model for low mach number combustion simulation, Combust Flame 209 (2019) 394–404.
[29] Y.Z. Liu, J. Xia, K.D. Wan, L. Vervisch, Z.H. Wang, H. Zhao, K.F. Cen, Simulation of char-pellet combustion and sodium release inside porous char using lattice Boltzmann method, Combust. Flame 211 (2020) 325–336.
[30] T.M. Lei, Z. Wang, K.H. Luo, Study of pore-scale coke combustion in porous media using lattice Boltzmann method, Combust. Flame 225 (2021) 104–119.
[31] C.G. Aguilar-Madera, O. Cazarez-Candia, G. Rojas-Altamirano, Oxygen transport in a matrix-fracture system under reactive conditions at pore-scale, J. Pet. Sci. Eng. 130 (2015) 96–105.
[32] Y.L. Feng, M. Tayyab, P. Boivin, A lattice-Boltzmann model for low-Mach reactive flows, Combust. Flame 196 (2018) 249–254.
[33] T.M. Lei, K.H. Luo, Pore-scale study of dissolution–driven density instability with reaction $A + B \rightarrow C$ in porous media, Phys. Rev. Fluids 4 (6) (2019) 063907.
[34] Y. Ren, N.P. Freitag, N. Mahinpey, A Simple Kinetic Model for Coke CombustionDuring an In Situ Combustion (ISC) Process, in: Canadian International Petroleum Conference, OnePetro, 2005.
[35] M. Cinar, L.M. Castanier, A.R. Kovscek, Combustion kinetics of heavy oils in porous media, Energy Fuels 25 (10) (2011) 4438–4451.